Energetic Magnetosheath Ions Connected to the Earth's Bow Shock: Possible Source of CEPs

20 December 2001

Prepared by

S.-W CHANG,[1] J. D. SCUDDER,[1] J. F. FENNELL,[2]
R. FRIEDEL,[3] R. P. LEPPING,[4] C. T. RUSSELL,[5]
K. J. TRATTNER,[6] S. A. FUSELIER,[6]
W. K. PETERSON,[6] and H. E. SPENCE[7]

[1]Department of Physics and Astronomy, University of Iowa, Iowa City
[2]The Aerospace Corporation, Los Angeles, CA
[3]Los Alamos National Laboratory, Los Alamos, NM
[4]NASA Goddard Space Flight Center, Greenbelt, MD
[5]Institute of Geophysics and Planetary Physics University of California,
    Los Angeles
[6]Lockheed Martin Advanced Technology Center, Palo Alto, CA
[7]Center for Space Physics, Boston University, Boston, MA

Prepared for

SPACE AND MISSILE SYSTEMS CENTER
AIR FORCE SPACE COMMAND
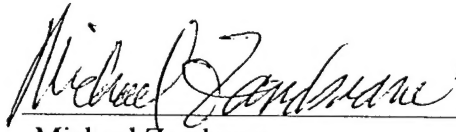2430 E. El Segundo Boulevard
Los Angeles Air Force Base, CA 90245

Engineering and Technology Group

THE AEROSPACE
CORPORATION
El Segundo, California

Michael Zambrana
SMC/AXE

REPORT DOCUMENTATION PAGE

Public reporting burden for this collection of information is estimated to average 1 hour per response, including the time for reviewing instructions, searching existing data sources, gathering and maintaining the data needed, and completing and reviewing this collection of information. Send comments regarding this burden estimate or any other aspect of this collection of information, including suggestions for reducing this burden to Department of Defense, Washington Headquarters Services, Directorate for Information Operations and Reports (0704-0188), 1215 Jefferson Davis Highway, Suite 1204, Arlington, VA 22202-4302. Respondents should be aware that notwithstanding any other provision of law, no person shall be subject to any penalty for failing to comply with a collection of information if it does not display a currently valid OMB control number. **PLEASE DO NOT RETURN YOUR FORM TO THE ABOVE ADDRESS.**

1. REPORT DATE (DD-MM-YYYY) 20-12-2001	2. REPORT TYPE	3. DATES COVERED (From - To)

4. TITLE AND SUBTITLE

Energetic Magnetosheath Ions Connected to the Earth's Bow Shock: Possible Source of CEPs

5a. CONTRACT NUMBER
F04701-00-C-0009

5b. GRANT NUMBER

5c. PROGRAM ELEMENT NUMBER

6. AUTHOR(S)

S.-W Chang, J. D. Scudder, J. F. Fennell, R. Friedel, R. P. Lepping, C. T. Russell, K. J. Trattner, S. A. Fuselier, W. K. Peterson, And H. E. Spence

5d. PROJECT NUMBER

5e. TASK NUMBER

5f. WORK UNIT NUMBER

7. PERFORMING ORGANIZATION NAME(S) AND ADDRESS(ES)

The Aerospace Corporation
Laboratory Operations
El Segundo, CA 90245-4691

8. PERFORMING ORGANIZATION REPORT NUMBER

TR-2000(8570)-3

9. SPONSORING / MONITORING AGENCY NAME(S) AND ADDRESS(ES)
Space and Missile Systems Center
Air Force Space Command
2430 E. El Segundo Blvd.
Los Angeles Air Force Base, CA 90245

10. SPONSOR/MONITOR'S ACRONYM(S)
SMC

11. SPONSOR/MONITOR'S REPORT NUMBER(S)
SMC-TR-02-06

12. DISTRIBUTION/AVAILABILITY STATEMENT

Approved for public release; distribution unlimited.

13. SUPPLEMENTARY NOTES

20020312 026

14. ABSTRACT

Plasma and magnetic field data detected by NASA GGS/POLAR and WIND during the May 4, 1998 storm event are analyzed to demonstrate for the first time a causal relation between the magnetosheath energetic ions and bow shock magnetic geometry. Intense magnetosheath energetic ions observed upstream from the cusp are from the quasi-parallel bow shock and show properties indicating that they are a possible source of cusp energetic ions (CEPs).

15. SUBJECT TERMS

Particle acceleration, Bow shock, Cusp

16. SECURITY CLASSIFICATION OF:			17. LIMITATION OF ABSTRACT	18. NUMBER OF PAGES	19a. NAME OF RESPONSIBLE PERSON Joe Fennell
a. REPORT UNCLASSIFIED	**b. ABSTRACT** UNCLASSIFIED	**c. THIS PAGE** UNCLASSIFIED		32	**19b. TELEPHONE NUMBER (include area code)** (310)336-7075

Acknowledgments

Contents

Plates

Figures

1. Introduction

Energetic ($\sim 10^1$-10^2 keV) ions are often observed in the magnetosheath. Two dominant sources are the magnetosphere [e.g., *Hones et al.*, 1972; *West and Buck*, 1976; *Sibeck et al.*, 1987; *Fuselier et al.*, 1991] and the solar wind energized at the bow shock [e.g., *West and Buck*, 1976; *Asbridge et al.*, 1978; *Crooker et al.*, 1981; *Fuselier et al.*, 1991]. To understand the origins of energetic magnetosheath ions would greatly facilitate the determination of the mass, momentum, and energy transfer processes within the geospace.

The escape of energetic magnetospheric particles into the magnetosheath at times occurs on interconnected magnetosphere-magnetosheath field lines that result from magnetic reconnection at the magnetopause [e.g., *Speiser et al.*, 1981; *Scholer et al.*, 1981]. However, it mostly occurs on a continuous basis through a leakage process of finite gyroradius effects [*Sibeck et al.*, 1987]. This mechanism predicts that energetic ions leak from the magnetosphere at postnoon local times and energetic electrons at prenoon local times due to the difference in their drift paths in the magnetosphere. These ions stream along magnetosheath magnetic field lines. Depending on the magnetic geometry they may escape into the upstream region of the bow shock [e.g., *Sarris et al.*, 1976; *Luhmann et al.*, 1984].

The upstream and downstream regions of the quasi-parallel bow shock (the angle between the average upstream magnetic field and the shock normal, θ_{Bn}, less than 45°) are often populated with energetic particles and magnetic waves and turbulence [e.g., *Paschmann et al.*, 1979; *Greenstadt at el.*, 1980; *Bonifazi and Moreno*, 1981; *Crooker et al.*, 1981; *Ipavich et al.*, 1981; *Greenstadt*, 1985; *Luhmann et al.*, 1986; *Möbius et al.*, 1987; *Gosling et al.*, 1989; *Fuselier et al.*, 1995, and references therein]. Beginning with the earliest observations, it was realized that the connection of the interplanetary magnetic field (IMF) to the bow shock is a necessary condition for the presence of energetic particles on the field line [e.g., *Asbridge et al.*, 1968; *Scudder et al.*, 1973; *Lin et al.*, 1974]. The fact that the enhanced plasma and magnetic turbulence and their associated energetic ions are similar in both the upstream and downstream regions led to the suggestion of the same bow shock source region [e.g., *West and Buck*, 1976; *Asbridge et al.*, 1978]. The occurrence rate of enhanced energetic ion events increases with decreasing θ_{Bn} both upstream and downstream from the bow shock [e.g., *Bonifazi and Moreno*, 1981; *Mitchell and Roelof*, 1983; *Crooker et al.*, 1981]. It is widely accepted that solar wind ions undergo first-order Fermi acceleration by scattering back and forth across the quasi-parallel bow shock in the turbulent regions upstream and downstream from the shock [*Lee*, 1982; *Ellison*, 1985]. In-situ plasma and magnetic field observations have confirmed theoretical predictions of the coupling between the particles and waves [*Möbius et al.*, 1987; *Trattner et al.*, 1994]. Energy spectra of energetic ions

1

from computer simulations are also in a very good agreement with observations both upstream and downstream from the quasi-parallel shock [*Ellison et al.*, 1990]. Bursts of magnetospheric ions are also occasionally observed in the upstream region but they have a much harder spectrum than those of bow shock accelerated solar wind ions [*Möbius et al.*, 1986].

Ion composition measurements have played a critical role in determining the relative contribution of bow shock accelerated ions and leakage of magnetospheric ions to the magnetosheath energetic ions [e.g., *Fuselier et al.*, 1991]. The angular distribution of bow shock accelerated ions immediately downstream from the quasi-parallel bow shock is anisotropic with the maximum flux toward the magnetopause [e.g., *Scholer et al.*, 1989; *Ellison et al.*, 1990]. They contribute to the majority of energetic H^+ ($> 65\%$) and almost all the energetic He^{+2} in the magnetosheath downstream from the quasi-parallel shock [*Fuselier*, 1994]. Leakage of magnetospheric ions plays a minor role in this region but accounts for nearly all the energetic protons in the plasma depletion layer [*Fuselier*, 1992], a thin layer adjacent to the magnetopause just outside the magnetosphere in the magnetosheath [*Zwan and Wolf*, 1976].

Recent observations of cusp energetic particles (CEP's) suggest that they are from the bow shock accelerated ions [*Chang et al.*, 1998]. If this hypothesis is true, one would expect the appearance of bow shock accelerated ions in the magnetosheath upstream from the cusp. In this paper, we present evidence of magnetosheath energetic ions upstream from the cusp accelerated at the quasi-parallel bow shock using plasma and magnetic field data observed by the NASA GGS/POLAR and WIND spacecraft during a magnetic storm event on May 4, 1998. In contrast to previous statistical work [e.g., *Crooker et al.*, 1981; *Fuselier*, 1994], it is demonstrated for the first time a causal relation between the magnetosheath energetic ions and bow shock magnetic geometry. This storm provides a great opportunity to understand the source of magnetosheath energetic ions and to check the hypothesis of bow shock source of CEP's by suppling large-scale temporal variations in the energetic ion fluxes which should be correlated with upstream parameters at the source region with a proper time delay. With the high-time resolution data from POLAR and WIND, based on the aforementioned principle we are able to determine not only the origin of the observed magnetosheath energetic ions but also the upstream parameters that control the intensity of these ions.

The rest of the paper is organized as followed. In section 2, we present the instrumentation; section 3, POLAR observations of plasma composition and data interval selection for cross-correlation analysis; section 4, solar wind propagation time; section 5, magnetosheath energetic ions and their correlation with IMF cone angle; section 6, interpretation of the analysis results; and section 7 summary and conclusions.

2. Instrumentation

Energetic ion composition measurements during this storm event were from the Magnetospheric Ion Composition Sensor (MICS) of the Charge and Mass Magnetospheric Ion Composition Experiment (CAMMICE) onboard POLAR. A similar detector was flown on the CRRES satellite [*Wilken et al.*, 1992]. The MICS sensor sampled 2-D angular distributions and covered the energy range from 1 to 193.4 keV/e for H^+ and He^{+2}, 1 to 100.1 keV/e for $O^{>+2}$, and 41.1 to 193.4 keV/e for $O^{<+3}$. It took about 3.3 min to complete a full energy sweep. The H^+ data were the total ion measurements assuming H^+ response in the Double Coincidence Rate (DCR) channel of the MICS detector. The detector viewed perpendicular to the spacecraft spin axis which was mainly in the dawn-dusk direction during this event. Energetic electron observations were from the Imaging Electron Sensor (IES) of the Comprehensive Energetic Particle and Pitch Angle Distribution (CEPPAD) onboard POLAR [*Blake et al.*, 1995]. The sensor sampled 3-D distributions covering the energy range from 12 to 400 keV. The lower energy part of the ion spectrum was provided by the Hydra spectrometer [*Scudder et al.*, 1995] which sampled 3-D distributions of electrons and ions (assuming H^+) covering the energy range from about 10 eV to 19 keV. The electron measurements from Hydra as well as the magnetic field measurements from the Magnetic Field Experiment (MFE) magnetometer [*Russell et al.*, 1995] were used to identify regions of plasma sheet, magnetopause boundary layer, magnetosheath, and solar wind along the POLAR trajectory. Upstream solar wind and IMF data were acquired with the Magnetic Field Investigation (MFI) magnetometer [*Lepping et al.*, 1995] and the Faraday cup of the Solar Wind Experiment (SWE) [*Ogilvie et al.*, 1995] both onboard the WIND spacecraft.

3. Overview of POLAR Observations

On May 4, 1998, 0500-1200 UT, the POLAR spacecraft was moving from $-0.3°$ to $74.1°$ magnetic latitude and from 4.4 to 9.0 R_E geocentric distance near the magnetic local noon. The WIND spacecraft was about 214 R_E upstream from the Earth, just north of the Sun-Earth line. A very strong interplanetary shock arrived at WIND at about 0230 UT. WIND observed large variations in the solar wind density ($\sim$4-65 cm^{-3}) and IMF strength ($\sim$5-40 nT) and high solar wind bulk speed $\sim$800 km/s for the next 9 hours. Because of high solar wind dynamic pressure (as large as 65 nP), magnetosphere was severely compressed and bow shock even reached the POLAR altitude on several occasions. As a result of the rapid boundary motion due to the dynamics of the storm, POLAR frequently crossed the magnetopause current layer. However, POLAR was in the high-latitude dayside magnetosheath most of the time during the second half period of the storm event. (Note only relevant POLAR data are presented here to address the plasma composition and magnetosheath interval selection for the cross-correlation

analysis. For detailed analysis of POLAR observations for this event see *Scudder et al. (AND/OR OTHERS?)* [1999d].)

Plate 1 presents from top to bottom panels MFE magnetic field magnitude, energy-time spectrograms for CAMMICE/MICS $O^{<+3}$, $O^{>+2}$, He^{+2}, DCR-H^+, Hydra ions, CEPPAD/IES electrons, and Hydra electrons from 0500 to 1200 UT. The total energy coverages for H^+ and electron are ~0.02-200 keV and ~0.01-400 keV, respectively. Before 0525 UT, POLAR was in the plasma sheet characterized by a large magnetic field (> 220 nT) dominated by the positive B_z component, and relatively intense energetic $O^{<+3}$ (> 40 keV/e), H^+ (> 40 keV), and electrons (> 20 keV) but relatively weak lower-energy (below 40 keV/e) $O^{>+2}$, He^{+2}, and H^+ fluxes. POLAR then moved into the low-latitude boundary layer (LLBL) and observed similar features before it exited the magnetopause into the magnetosheath at about 0541 UT [*Russell et al.*, 1999]. Although the plasma sheet and LLBL are both on closed magnetic field lines with both feet anchored to the Earth, electron pitch angle distributions there are somewhat different, trapped population in the former region and counter-streaming distribution in the latter.

By contrast, in the magnetosheath from ~0541 to ~0610 UT POLAR observed disturbed weak magnetic field, enhanced $O^{>+2}$, He^{+2}, H^+ and 1-keV ions and 100-eV electrons but weak $O^{<+3}$ and energetic electron flux (both nearly close to the background values). Then POLAR moved into the LLBL again. During the early part of the storm event from 0500 to 0730 UT, POLAR was moving back and forth between the magnetosheath and the plasma sheet/LLBL across the magnetopause. After 0730 UT, POLAR was in the magnetosheath and encountered the bow shock for the first time at about 0735 UT. Due to the arrival of a brief, very strong pressure pulse (solar wind dynamic pressure ~65 nP) bow shock moved to 7.3 R_E at 38° magnetic latitude and 11 o'clock magnetic local time. POLAR briefly stayed upstream from the shock and observed very cold solar wind ions and electrons as shown in the Hydra ion and electron spectrograms in Plate 1. It encountered bow shock several times after that.

The bow shock crossings are more obviously illustrated in Figure 1 which shows the magnitude of the magnetic field from MFE and electron density from Hydra covering 0730-1000 UT. Bow shock crossings are identified by the simultaneous, abrupt jumps in the two quantities. In addition electron bulk speed and temperature jumps also occurred corresponding to the magnetic field and electron density jumps. As POLAR moved from the magnetosheath across the strong shock into the upstream region, a sharp increase in the electron bulk speed and a sharp decrease in the magnetic field, electron temperature and density occurred, and vice versa [*Scudder et al. (AND/OR OTHERS?)*, 1999c]. Several upstream regions from the bow shock are identified and marked as the shaded regions in Figure 1. As the solar wind dynamic pressure quickly reduced, the bow shock and magnetopause retreated toward their normal positions and
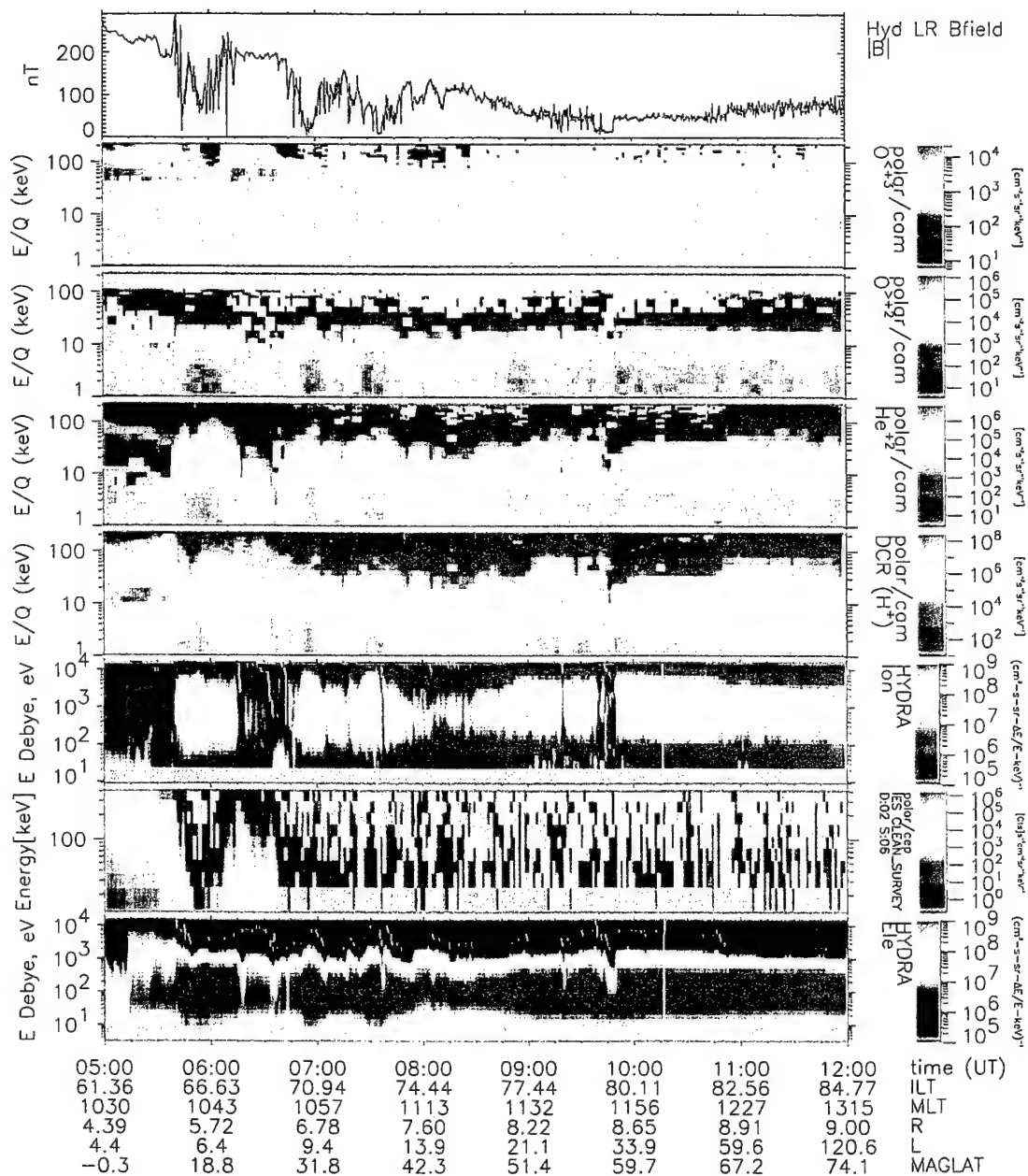
Plate 1. Magnetic field and plasma measurements from four instruments onboard PO-LAR from 5 to 12 UT on May 4, 1998: from top to bottom, MFE magnetic field magnitude, energy-time spectrograms for CAMMICE/MICS $O^{<+3}$, $O^{>+2}$, He^{+2}, DCR-H$^+$, Hydra ions, CEPPAD/IES electrons, and Hydra electrons. Distinct features were apparent as POLAR traversed various regions between the plasma sheet and upstream region of the bow shock.

POLAR crossed the magnetopause into the magnetopause boundary layer at about 0755 UT. Electron temperature then increased as expected.

The best signature however for distinguishing the boundary layer and magnetosheath region is the electron distribution since two regions have distinct magnetic topology, one for a closed magnetic field line and the other for a magnetosheath field line which is connected to IMF and may or may not be connected to a geomagnetic field line. As an example shown in Figure 2a, electrons commonly show a counter-streaming distribution in the boundary layer, indicating a closed magnetic topology. Another very useful diagnostic of the magnetopause current layer as a rotational discontinuity is the generalized Walén test [Scudder et al., 1999a]. Magnetopause crossings identified using this technique are consistent with the findings based on the electron distributions [Scudder et al. (REFERENCE?), 1999b]. After 0755 UT, POLAR frequently crossed the magnetopause before exiting the boundary layer at ~0836 UT. After that, except several brief upstream regions from the bow shock, POLAR was in the magnetosheath until the end of the magnetic storm at about 1200 UT. The common electron distribution in the magnetosheath is nearly isotropic, accompanied by a weak field-aligned beam at low energy as shown in Figure 2b.

As shown in Plate 1, ion composition of energetic ions ($O^{<+3}$, $O^{>+2}$, He^{+2}, and H^+) shows a distinct relative abundance in the plasma sheet and magnetosheath. Magnetosheath energetic ions are likely of the solar wind origin. During this storm event, the magnetosheath energetic ion fluxes show lots of variations (see for example 50 keV/e ions in the third to the fifth panel of Plate 1). Energetic ion fluxes observed upstream in the solar wind by the 3D Plasma instrument [Lin et al., 1995] onboard WIND on the other hand were quite uniform. In addition, these fluxes are about 1 to 3 orders of magnitude lower than the magnetosheath energetic ion fluxes observed by POLAR. Therefore, the solar energetic particles can not be a direct source of the POLAR observations. To understand the cause of the variations and ultimately the origin of these magnetosheath energetic ions, we choose the later, long period of magnetosheath interval (0840-1200 UT excluding upstream intervals) for systematic analysis.

4. Solar Wind Propagation Time

If the source of the magnetosheath energetic ions is at a distance, the timing for the transport is a crucial factor. Since their composition suggests a solar wind source, solar wind propagation time becomes the next obvious quantity to examine. The propagation time can be estimated by four different methods utilizing the plasma and field measurements from WIND and POLAR. The first simple estimate is to use the measured solar wind bulk speed from WIND/SWE which was quite uniform ~770 km/s

6

UT	07:30	08:00	08:30	09:00	09:30	10:00
ILT	72.77	74.44	75.99	77.44	78.81	80.11
MLT	1105	1113	1122	1132	1143	1156
R	7.22	7.60	7.93	8.22	8.45	8.65
L	11.4	13.9	17.1	21.1	26.6	33.9
MLAT	37.3	42.3	47.0	51.4	55.6	59.7
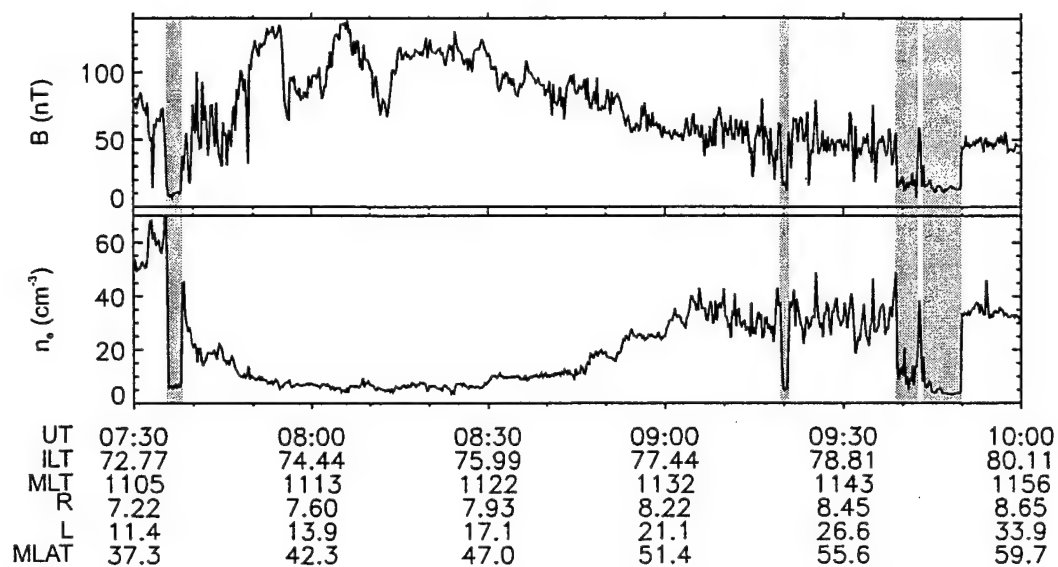
Figure 1. POLAR/MFE magnetic field magnitude and Hydra electron density from 0730 to 1000 UT. POLAR was mainly in the dayside magnetosheath and briefly crossed the bow shock into the upstream region (shaded) several times as indicated by the simultaneous, abrupt jumps in the two quantities.
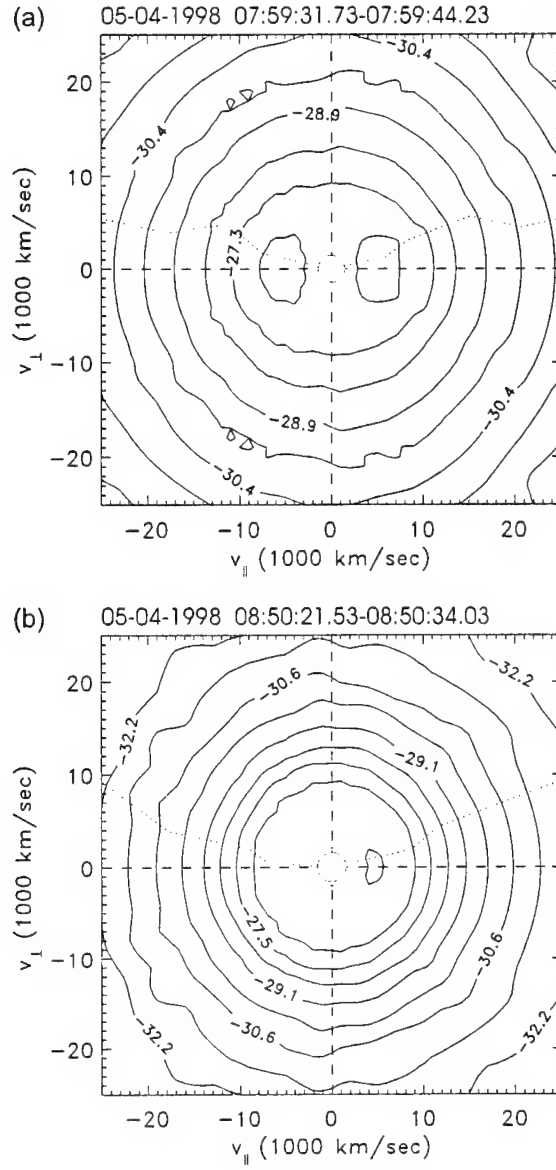
Figure 2. Contours of constant phase space density for electrons from POLAR/Hydra in the plane of velocity components perpendicular and parallel to the magnetic field, showing (a) a counter-streaming distribution at energies below ~500 eV in the magnetopause boundary layer and (b) a nearly isotropic distribution with a weak field-aligned beam at ~60 eV in the magnetosheath.

from 0650 to 0730 UT. Estimated propagation time is 28 min for solar wind traveling a distance of 204 R_E from WIND to bow shock.

The POLAR magnetic field profile observed in the upstream region of the bow shock from 0735:47 to 0738:03 UT is unique to the WIND IMF data set so that a comparison of IMF measurements from two spacecraft can give a fairly accurate estimate of the solar wind propagation time. Figure 3 presents the magnetic field measurements from POLAR/MFE and WIND/MFI offset 27.3 min. The scales of all the vertical axes are set to facilitate the comparison and therefore most of the POLAR measurements are out of scale. In the upstream region, B_x and B_z components from POLAR both turned from positive to negative at about the same time. An identical feature was also observed by WIND about 27.3 min ahead. All the three components and magnitude of IMF from POLAR and WIND (shaded region) match very well, with the exception of the B_y components which show different trends but maintain the same sign. Within 2 hours ahead of this POLAR upstream interval, only one match for all three IMF components occurs in the WIND data set. Other intervals have at best a match in one component only. The solar wind propagation time from WIND to POLAR just upstream from the bow shock is thus 27.3 min consistent with the estimate from the solar wind bulk speed. For the time interval of interest, 0810-1130 UT, corresponding to the interval of the POLAR magnetosheath energetic ion observations, the solar wind bulk speed decreased to about 755 km/s which gives an estimate of the propagation time of ~29 min from WIND to bow shock. Additional several minutes are required for plasmas to propagate from the shock to POLAR in the magnetosheath because bow shock decelerates the flow.

Since magnetosheath magnetic field lines are connected to the IMF, magnetosheath field and IMF to some extent would be correlated despite magnetic field being modified by the electric current at bow shock. Figure 4 presents the three magnetic field components observed by POLAR from 0840 to 1200 UT and by WIND with a lag indicated in each panel. These lags are determined by a cross-correlation analysis of the POLAR and WIND observations during the above interval excluding the upstream regions from bow shock (shaded regions in the figure). Correlation coefficient for each magnetic field component is calculated for a lag from 0 to 60 min. All three correlation coefficient curves show one unique peak with the correlation coefficients (0.94, 0.46, 0.73) and time lags (35, 34, 37) min for B_x, B_y, and B_z, respectively. Strong correlation appears in B_x, good correlation in B_z but weak correlation in B_y, as illustrated in the figure. From these results, the estimated plasma propagation time from WIND to POLAR is approximately 35-37 min which is consistent with the estimate using the solar wind bulk speed and magnetosheath plasma flow speed.

Another estimate of the propagation time is given by the cross-correlation analysis of the solar wind density and magnetosheath plasma density. Figure 5 presents electron
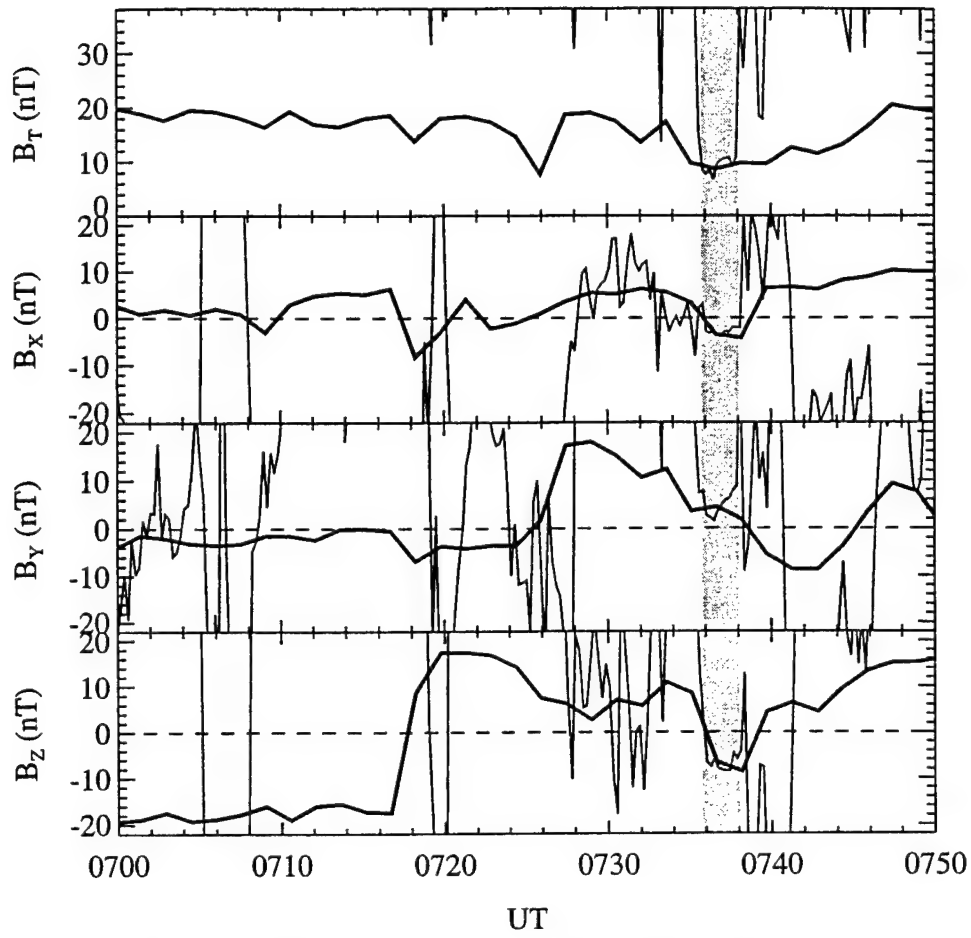
Figure 3. Magnitude and three GSM components of magnetic field observed by PO-LAR/MFE (thin) from 0700 to 0750 UT and WIND/MFI (thick) in the solar wind offset 27.3 min. The IMF profile from POLAR just upstream from the bow shock (shaded interval) matches the WIND observations very well. The scales of the vertical axes are set for an easy comparison of IMF profiles. Therefore, MFE measurements are off scale most of the time.
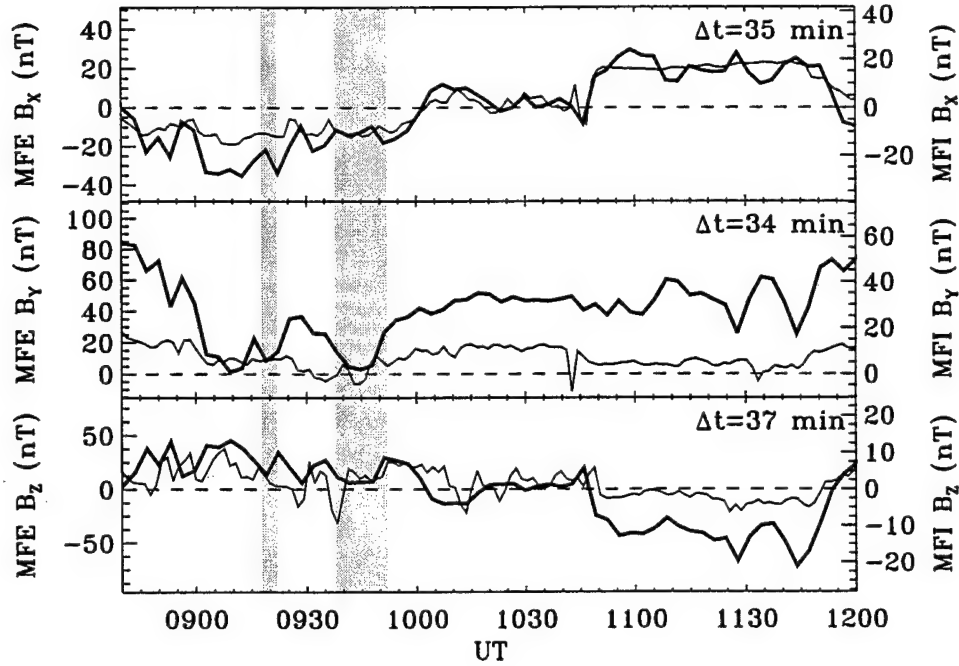
Figure 4. GSM magnetic field components in the magnetosheath from POLAR/MFE (thick) from 0840 to 1200 UT and IMF components from WIND/MFI (thin) offset by a Δt. The Δt in each panel is the time delay associated with the peak correlation between the magnetosheath magnetic field and IMF. Intervals of shaded areas are excluded in the cross-correlation analysis. Very strong correlation appears in B_x, good correlation in B_z but weak correlation in B_y. Estimated solar wind propagation time is $\sim$ 35-37 min.

density from POLAR/Hydra from 0840 to 1200 UT and solar wind proton density from WIND/SWE offset 33 min. The upstream regions (shaded) are again excluded in the analysis. As expected, magnetosheath plasma density is strongly correlated with the solar wind density with a proper time delay. The correlation coefficient as a function of the lag from 0 to 60 min once again demonstrates a unique peak value of 0.85 at a lag of 33 min, yielding another estimate of the solar wind propagation time. This peak however is not as sharp as those in the analysis of the magnetosheath magnetic field and IMF B_z and B_x components presented above. Therefore, there is a somewhat larger uncertainty (± 3 min) in the estimate. Nevertheless, the estimated propagation time is consistent with the one based on the magnetic field comparison.

5. Magnetosheath Energetic Ions

Figure 6 depicts energy spectra of H^+, He^{+2}, and $O^{>+2}$ from Hydra and CAMMICE in the magnetosheath, averaged over an interval from $\sim$0840 to $\sim$1200 UT excluding the solar wind intervals. Ion fluxes are plotted against the ion energy per charge. In this format, spectral shapes for all three species are similar. In particular, they are nearly identical for H^+ and He^{+2} with energy above 20 keV/e. Some differences in $O^{>+2}$ are due to very low count rates which create much larger errors in the counting statistics. It gets worse as $O^{>+2}$ energy gets higher. Nevertheless, all three spectra are continuous with a spectral break at about 41.1 keV/e. These spectra resemble those upstream and downstream from the quasi-parallel bow shock (cf. Figures 3 and 4 of *Möbius et al.* [1987] and Figure 2 of *Ellison et al.* [1990]). It is noted that there are substantial variations in the ion fluxes during this magnetosheath interval. Ion spectra of the highest time resolution (3.3 min) would move up and down along the vertical axis in Figure 6 as time steps through each interval of full energy sweep within the above magnetosheath interval but their spectral shapes remain similar.

To examine the hypothesis of the observed magnetosheath energetic ions, especially ions with energy above the spectral break, originated from the bow shock accelerated ions, a cross-correlation analysis of the magnetosheath H^+ flux integrated from 41.1 to 193.4 keV/e and the IMF cone angle θ_{Bx} (the angle between the IMF and Sun-Earth line) was performed. Figure 7a presents the integrated H^+ flux at the highest time resolution from 0840 to 1200 UT and θ_{Bx} offset 36 min. Both quantities show large temporal variations, the maximum to minimum flux ratio $\sim$100 and $\theta_{Bx} \sim 10°-90°$. In addition, H^+ flux increases as θ_{Bx} decreases, and vice versa. Two quantities are strongly anti-correlated with a correlation coefficient of -0.82.

The correlation coefficient for the energetic ion flux and θ_{Bx} during this magnetosheath interval in general depends on the time lag for θ_{Bx} as shown in Figure 7b. As the time lag increases from 0 to 60 min, correlation coefficient starts at about

12
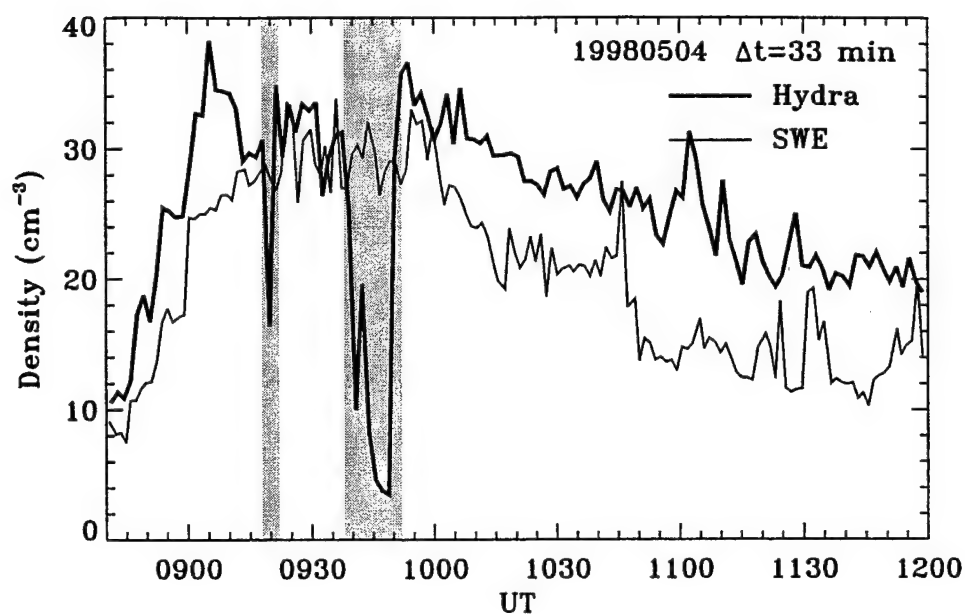
Figure 5. POLAR/Hydra electron density in the magnetosheath (thick) from 0840 to 1200 UT and the solar wind proton density from WIND/SWE (thin) offset 33 min. Two quantities are strongly correlated. The 33-min lag associated with the best correlation gives an estimate of the solar wind propagation time. Intervals of shaded areas are excluded in the cross-correlation analysis.
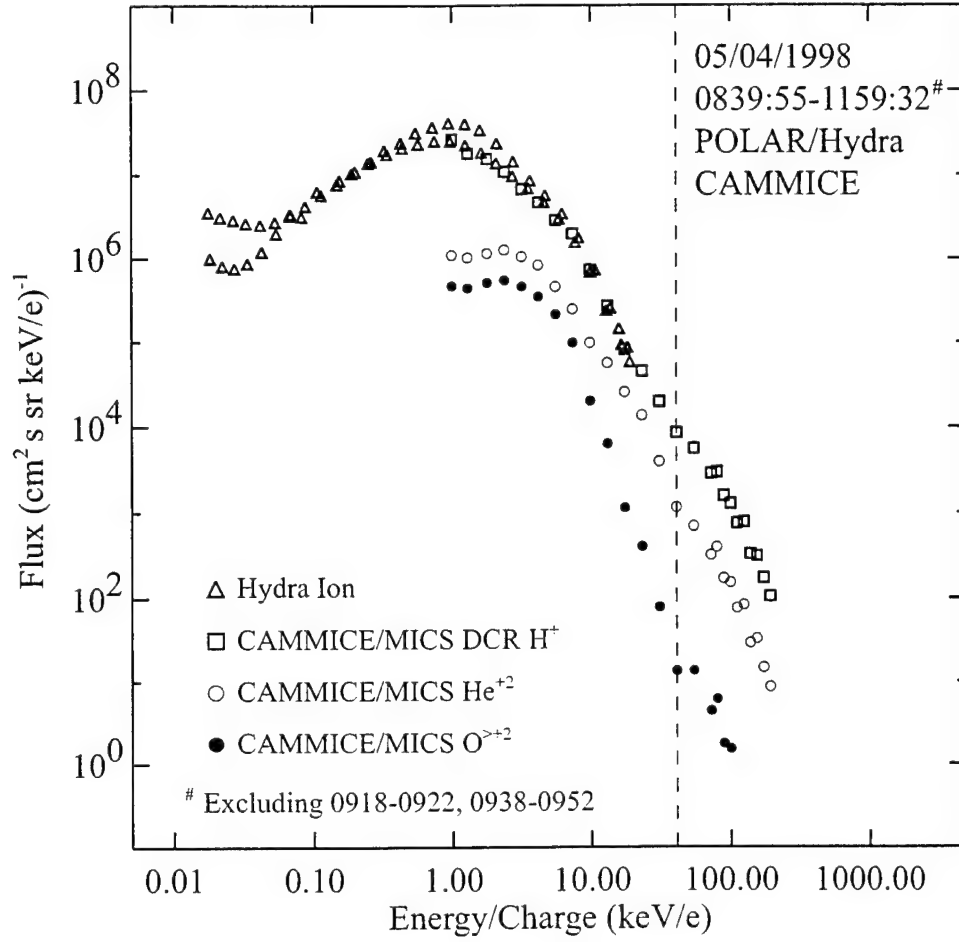
Figure 6. Energy spectra of magnetosheath H^+, He^{+2}, and $O^{>+2}$ from POLAR/Hydra and CAMMICE averaged over the interval ~0840-1200 UT excluding the solar wind intervals. Spectral shapes are similar, ordered by the ion energy per charge. They are nearly identical for H^+ and He^{+2} with energy above 20 keV/e. Some differences in $O^{>+2}$ are due to low count rate. Spectra are continuous with a spectral break at ~41.1 keV/e (vertical dashed line).

0, monotonically decreases, reaches the peak value -0.82 at 36-min lag, and then monotonically increases toward 0. This 36-min lag associated with the best correlation is consistent with the estimated solar wind propagation time and other time estimates (see discussions below).

Although all three ion spectra in Figure 6 are continuous with a spectral break at the same energy, lower- and higher-energy ions demarcated by this energy have distinct properties with respect to θ_{Bx}. Similar to the format in Figure 7b, correlation coefficients for the magnetosheath ion flux integrated from E_1 to E_2 and θ_{Bx} plotted against the time lag from 0 to 60 min are presented in Plate 2 for three ion species (H^+, He^{+2}, $O^{>+2}$), where E_1 steps through the detector energy channel from 1.0 to 100.1 keV/e and E_2 is fixed at the highest detector energy channel, 193.4 keV/e for H^+ and He^{+2} and 100.1 keV/e for $O^{>+2}$. These correlation curves are color coded according to their E_1's given in the color bar. The first most remarkable result is that all the curves at $E_1 \geq 41.1$ keV/e (in blue) from panels a and b are nearly identical. In addition, these curves have a unique peak correlation coefficient ~ -0.8 at a time lag of $\sim$36-37 min, suggesting that magnetosheath energetic (≥ 41.1 keV/e) H^+ and He^{+2} ion flux are strongly anti-correlated with θ_{Bx}.

It is even more striking that correlation curves for H^+ and He^{+2} begin to change drastically by including ion fluxes from one or two energy channels below 41.1 keV/e. They become much flatter and closer to the line of null correlation as shown by the green curves in panels a and b. This result suggests a critical energy for the anti-correlation between the magnetosheath energetic ion flux and θ_{Bx}. As E_1 continues to decrease toward 1 keV/e, the correlation curves for H^+ and He^{+2} begin to show some positive correlation and then move toward weak correlation as indicated by the yellow and red curves. Because energetic $O^{>+2}$ ions have very low count rates, correlation curves are rather irregular as shown in panel c. Nevertheless, these curves show a trend similar to those for H^+ and He^{+2}. Furthermore, at lower energies $O^{>+2}$ ions gain enough counting statistics so that correlation coefficient curves have more significance. These curves are nearly identical to those of He^{+2} at the same energies (cf. red curves in panels b and c).

To illustrate the strong energy dependence in the correlation coefficient, the peak correlation coefficient r_o is plotted against E_1 for all three ion species as shown in Figure 8a. It is clearly demonstrated that a critical energy E_c has to be reached for ion flux to be anti-correlated with θ_{Bx}. This critical energy equals to 41.1 keV/e for all three ion species and is exactly identical to the one at the spectral break suggested by Figure 6. Furthermore, r_o's are nearly constant for E_1 above E_c, ~ -0.82 for both H^+ and He^{+2} and ~ -0.71 for $O^{>+2}$. However when E_1 is above 70 keV/e, r_o begins to move toward 0 due to less significance in the ion counting statistics. This trend is more obvious for higher-energy $O^{>+2}$ since their fluxes are nearly close to the background value. Nonetheless, the sharp transition from strong anti-correlation to moderate
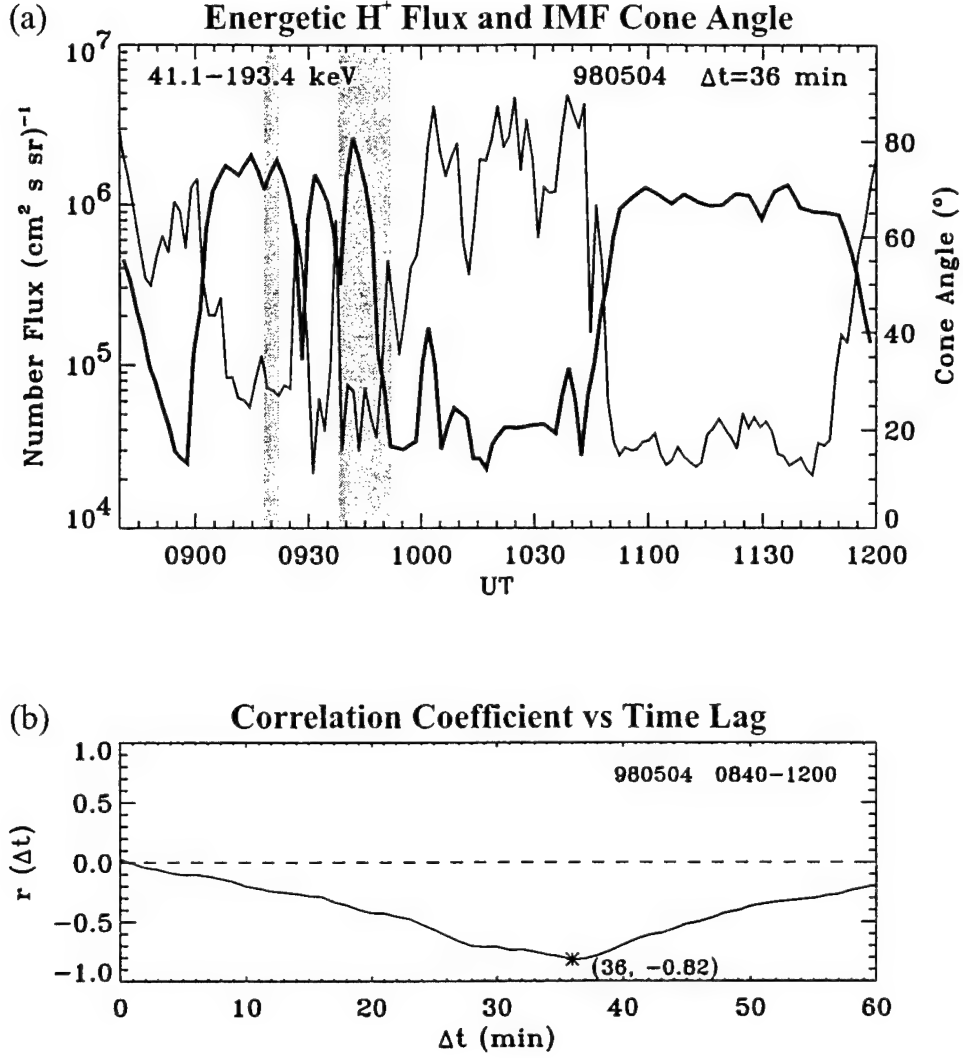
Figure 7. (a) Energetic ($41.1 \leq E \leq 193.4$ keV) H^{+} ion flux (thick line) from PO-LAR/CAMMICE in the interval 0840-1200 UT and θ_{Bx} (thin line) from WIND/MFI offset 36 min. Both show large temporal variations and are strongly anti-correlated. (b) The correlation coefficient is a function of the time lag. As time lag increases from 0 to 60 min, the correlation coefficient starts at about 0, monotonically decreases, reaches the peak value -0.82 at a lag of 36 min, and then monotonically increases toward 0. Note that the shaded intervals are excluded in the calculation of the correlation coefficient.

16
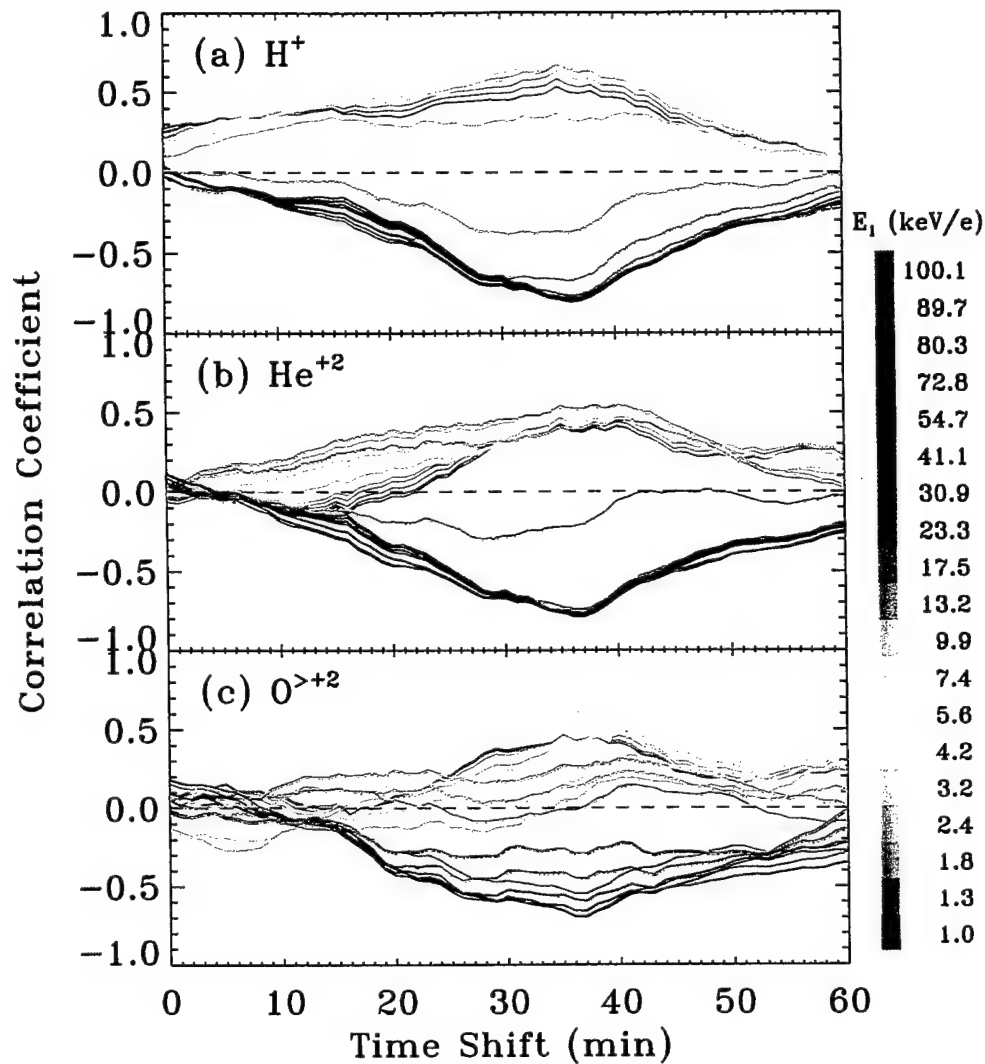
Plate 2. Correlation coefficient curves of the magnetosheath ion flux ($E_1 \leq E \leq E_2$) and θ_{Bx} for three ion species, (a) H$^+$, (b) He^{+2}, and (c) O$^{>+2}$. Curves are color coded according to their E_1's given in the color bar with E_2 equal to 193.4 keV/e for H$^+$ and He^{+2} and 101.1 keV/e for O$^{>+2}$. All the curves of H$^+$ and He^{+2} with $E_1 \geq 41.1$ keV/e (in blue) are nearly identical, showing a strong anti-correlation between the ion flux and θ_{Bx} offset 36–37 min (peak correlation coefficient ~ -0.8). Below 41.1 keV/e, curves sharply shift toward weakly positive correlation (in red). Similar trends also appear in O$^{>+2}$.

positive correlation just below E_c is vividly illustrated.

The time lag Δt_o associated with the peak correlation can be quite different for different energies as shown in Figure 8b. However when r_o is very small (< -0.7), Δt_o is nearly the same for all three ions at about 36-37 min. This Δt_o suggests a unique signal transmission time independent of ion energy and species. Results of the cross-correlation analysis for all three ions have demonstrated that magnetosheath energetic ions with energy above the spectral break are strongly anti-correlated with θ_{Bx} offset by a lag consistent with the solar wind propagation time and other time estimates that will be discussed later. This correlation cannot be incidental. Results of r_o and Δt_o for lower-energy ($E_1 < 10$ keV/e) ions shown in Figure 8 on the other hand can only indicate average results for lower-energy ions and will be discussed more later.

Since the observed magnetosheath energetic ion fluxes are controlled by θ_{Bx}, one would expect they flow antisunward away from the bow shock. In this storm event, the magnetosheath magnetic field was most of the time close to the POLAR's spin axis so that CAMMICE detector only covered a limited range of pitch angle around 90°. However during the interval from ~0850 to 1000 UT, magnetosheath energetic ions have a nearly full coverage of pitch angle that can deduce their flow direction. Figure 9 presents the normalized angular distribution of energetic ion flux at the highest time resolution for H^+, He^{+2} (both $41.1 \leq E \leq 193.4$ keV/e), and $O^{>+2}$ ($41.1 \leq E \leq 101.1$ keV/e) in the spacecraft frame for three different intervals in the magnetosheath. Because the plasma flow speed in the POLAR spin plane is about 300 km/s corresponding to ~0.5 keV/e in energy for H^+ and He^{+2}, correction by the plasma flow for the above energetic ion distributions is expected to be very small. Therefore, Figure 9 is a very good approximation of the energetic ion distributions in the rest frame of plasma.

As shown in Figure 9b and c, almost all the H^+ and He^{+2} in the magnetosheath proper and near the bow shock have pitch angles less than 90° with the maximum flux occurring at about 45° pitch angle. Therefore these ions show a strong flow along the magnetic field direction. During the interval covered in Figure 9a, POLAR was in the magnetosheath close to the magnetopause and energetic ions with pitch angles within 30° to the magnetic field line were not sampled. Nevertheless the observed partial angular distributions for H^+ and He^{+2} in this region are consistent with those observed in the magnetosheath proper and near the bow shock. As mentioned several times before, energetic $O^{>+2}$ ions are tenuous that is more apparent in this diagram. However, their angular distributions show a trend similar to those of the other two species.

Within the above magnetosheath interval (0850-1000 UT), the angular distributions of energetic ions are basically the same as those presented in Figure 9, showing a predominant flow along the magnetic field direction. Meanwhile the magnetosheath magnetic field B_x component turned negative and B_z turned positive after 0840 UT
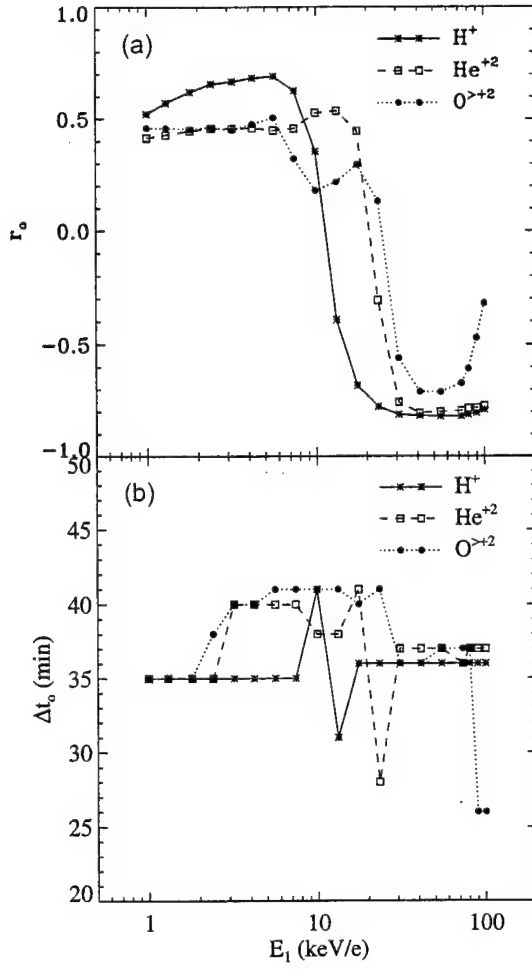
Figure 8. (a) Peak correlation coefficient r_o as a function of energy E_1 for three ion species. For $E_1 \geq E_c = 41.1$ keV/e, r_o's are nearly the same, ~ -0.82 for both H^+ and He^{+2} and ~ -0.71 for $O^{>+2}$. For E_1 above 70 keV/e, r_o's turn toward 0 due to lower count rate especially in $O^{>+2}$. A sharp transition from strong anti-correlation to weakly positive correlation occurs at energy immediately below E_c. This critical energy E_c happens to be the energy at the spectral break suggested by Figure 6. (b) Time lag associated with the peak correlation Δt_o as a function of energy E_1. In general Δt_o can be quite different. All the points of large negative r_o's (< -0.7) with $E_1 \geq E_c$ however have $\Delta t_o = 36\text{-}37$ min.

and maintained the same polarity until ~1002 UT as shown in Figure 4. Therefore the observed magnetosheath energetic ions during the above interval were streaming antisunward and northward away from the bow shock.

6. Discussions

In the previous section we have presented plasma and magnetic field measurements from the NASA GGS/POLAR and WIND satellites for the May 4, 1998 storm event. Here we discuss origin of the observed magnetosheath energetic ions based on possible explanations in the literature. In general two major sources are the solar wind and magnetospheric plasmas but the acceleration region and the transport can be quite different for each of the sources. Energetic magnetospheric ions in the plasma sheet on closed field lines can leak into the magnetosheath [e.g., *Sibeck et al.*, 1987]. Their intensity is more related to substorm activities in the magnetotail. Energetic ions previously on closed field lines can escape the magnetosphere into the magnetosheath along open field lines either by gradient and curvature drift across field lines or magnetic reconnection [e.g., *Scholer et al.*, 1981]. Solar energetic particles can also directly contribute to the magnetosheath energetic ions. Diffuse ions accelerated at the quasi-parallel bow shock can be another source [e.g., *West and Buck*, 1976; *Fuselier et al.*, 1991].

The composition of the observed magnetosheath energetic ions suggest they are ultimately from the solar wind not from the ionosphere. It is a question whether keV ions of solar wind origin entered the magnetosphere, convected to the magnetotail, were accelerated there and injected to the dayside, and then escaped the magnetosphere. Because the dayside plasma sheet and magnetosheath traversed by POLAR during this event show distinct energetic ion composition, leakage of magnetospheric ions is not likely a cause of the magnetosheath energetic ions. In addition, POLAR was on magnetosheath field lines which were most of the time connected to the solar wind, not the open magnetosphere (cusp, mantle, lobe, etc.). Escape of energetic ions through the open field lines is not a possible explanation for the observations. Most importantly magnetospheric source would have a difficulty to explain the fact that magnetosheath energetic ion flux of solar wind origin are anti-correlated with the IMF cone angle (θ_{Bx}).

Solar energetic ions observed by WIND are much less intense than the magnetosheath energetic ions during this event. Results of cross-correlation analysis reveal that both ion fluxes are slightly anti-correlated. Therefore solar energetic ions are not a direct source of magnetosheath energetic ions. However, an acceleration region at the bow shock can account for ions accelerated to hundreds of keV. As noted a long time ago, energetic ion spectra downstream from the shock are nearly identical to those in the upstream wave region (see for example Figure 10 of *West and Buck*

H⁺ He⁺² O^{>+2}

(a)

0843:18-0846:41

(b)

0903:36-0906:59

(c)

0913:45-0917:08
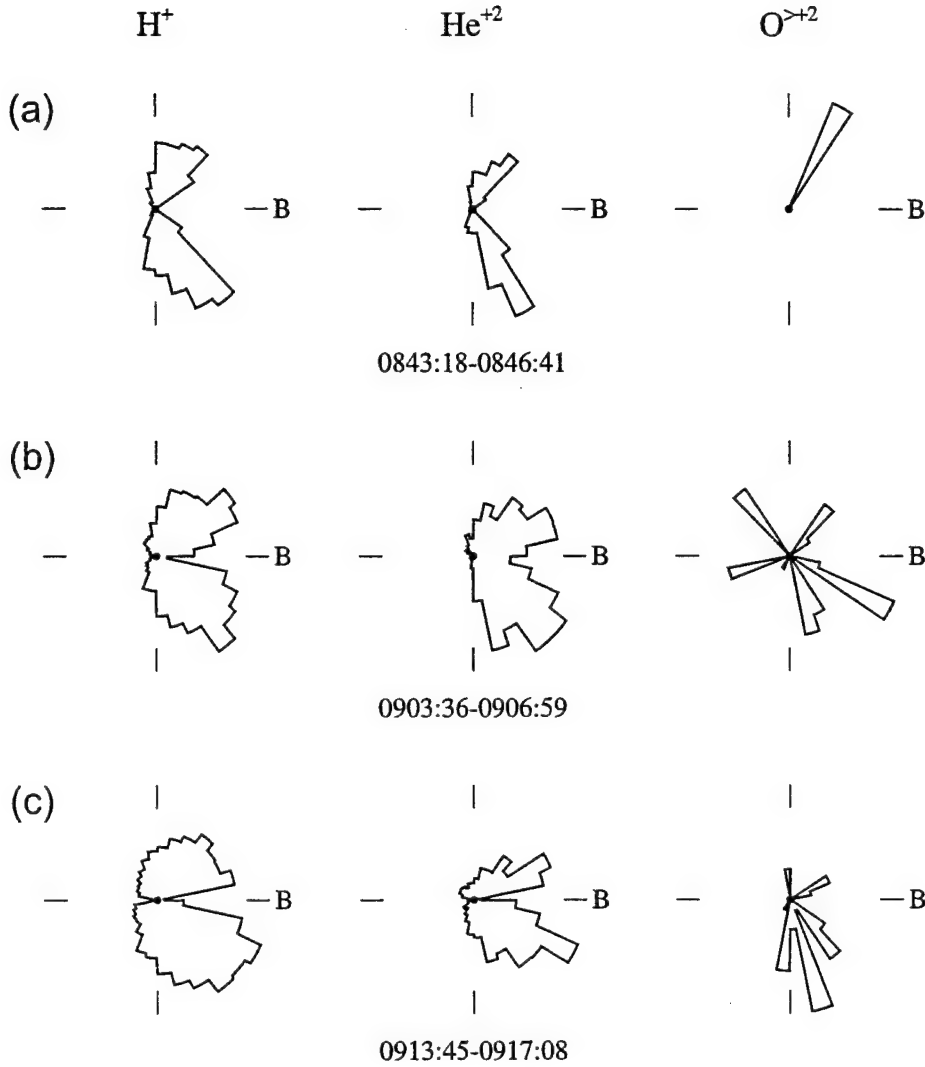
Figure 9. Normalized angular distribution of energetic ion flux for H^+, He^{+2} (both $41.1 \leq E \leq 193.4$ keV/e), and $O^{>+2}$ ($41.1 \leq E \leq 101.1$ keV/e) in the spacecraft frame for three intervals in the magnetosheath, (a) near the magnetopause boundary layer, (b) in the magnetosheath proper, and (c) near the bow shock. H^+ and He^{+2} ions are streaming along the magnetic field direction. Note that pitch angles within 30° to the magnetic field line in (a) are not sampled. Tenuous $O^{>+2}$ ions are apparent in this diagram but they show a trend consistent with the other two species.

[1976]). Ions undergo first-order Fermi acceleration by scattering back and forth across the quasi-parallel bow shock in the turbulent regions upstream and downstream from the shock. This mechanism is most efficient for highly charged ions [*Lee*, 1982]. The magnetosheath energetic ion spectra observed by POLAR have shown such a property.

Results of the cross-correlation analysis for the magnetosheath ion flux and θ_{Bx} are very striking. In order to lower the statistical error especially for higher-energy ions, we have done this analysis using the integrated ion number flux instead of the differential number flux at each MICS energy channel. Because of the steep drop in the energetic tail of the ion spectra, ion flux detected at the lowest energy channel in the integration energy range contributes most to the total flux. Therefore the integrated flux for ion energy above ~ 10 keV/e to some extent truly reflects the behavior of the differential flux at the lowest energy as demonstrated by the sharp transition in Figure 8. In fact, the correlation coefficient curves for ion differential number flux at energy above ~ 10 keV/e are very similar to the corresponding ones for the integrated flux presented in Plate 2. On the other hand, for ion energy below 10 keV/e the ion differential energy flux at the lowest energy does not dominate the total flux because the ion flux at this energy is not large enough to compensate the reduced energy in the integration. Thus, results of correlation analysis including these ions presented here only represent average results rather than results for ions detected at the lowest energy channel within the integration. The correlation curves for the differential ion flux at energy below 10 keV/e become more erratic showing a trend toward null correlation with decreasing energy, unlike the smooth, asymptotic behavior shown in Figure 8. This result of little correlation is expected because keV magnetosheath ions mainly come from the subsolar bow shock along streamlines and the intensity of solar wind ions there is not related to the IMF or bow shock geometry.

The most remarkable feature in the results of the cross-correlation analysis is that the correlation coefficient is energy dependent. Correlation coefficients as a function of ion energy show a sharp transition at the same energy (precisely energy per charge) for all three ion species. Above this critical energy ion fluxes are strongly anti-correlated with θ_{Bx} and essentially little correlation for energy immediately below it. It is even more striking that this critical energy is identical to the energy at the spectral break of the ion spectra. All the above results are consistent with the Fermi acceleration process since it is responsible for the energetic ions above the spectral break [e.g., *Lee*, 1982]. This process takes place at the quasi-parallel bow shock.

Statistical studies show that probability of enhanced energetic ion events upstream and downstream from the bow shock increases as θ_{Bn} decreases, and vice versa [*Mitchell and Roelof*, 1983; *Crooker et al.*, 1981]. In principle an appropriate θ_{Bn} should be used in the cross-correlation analysis. Since the observed magnetosheath energetic ions are extremely energetic, they are guided more or less by the magnetic field lines not the

flow streamlines in the subsonic medium [e.g., *Bonifazi and Moreno*, 1981; *Mitchell and Roelof*, 1983]. For example, a 41.1 keV/e H^+ or He^{+2} ion with a pitch angle of 45°, the velocity component parallel to the magnetic field is about 1900 km/s which is more than 4 times of the E × B drift speed observed in the magnetosheath. Because the associated θ_{Bn} where the magnetosheath magnetic field line through POLAR intersets the bow shock is not readily known, θ_{Bx} is used as a proxy for θ_{Bn}. Furthermore, θ_{Bx} and the angle between the IMF B_y and B_z components would completely determine the bow shock magnetic geometry.

Magnetosheath energetic ion fluxes are enhanced in two intervals, ∼9-10 and ∼11-12 UT. Figure 10 shows the average dayside bow shock surface projected onto the y-z plane for the first interval. This bow shock surface is based on the Fairfield model [*Fairfield*, 1971]. For the IMF observed by WIND associated with this interval, $(-13.3, 5.5, 5.5)$ nT, θ_{Bx} is 30.3° and the quasi-parallel shock as shown by the shaded region covers the majority portion of the southern hemisphere and part of the northern hemisphere of the dayside bow shock surface. During the second interval, IMF B_x and B_z components reverse the orientation and θ_{Bx} is further reduced to about 10°. The quasi-parallel bow shock switches to the east side and further expands, covering a great portion of the southern hemisphere and most of the northern hemisphere of the dayside bow shock surface. As for the interval of weak magnetosheath energetic ion fluxes, ∼10-11 UT, θ_{Bx} is about 80° and nearly the entire dayside bow shock surface is quasi-perpendicular. The quasi-parallel shock in this case occupys only a small portion of the dusk flank for IMF B_y positive.

The majority of magnetosheath energetic ions observed by POLAR have pitch angles about 45° (Figure 9). Thus, almost all the energetic ions with the exception of those with pitch angles nearly 90°, would tend to follow the magnetic field lines. During the first interval of the enhanced magnetosheath energetic ion flux, ∼9-10 UT, both IMF and magnetosheath magnetic field have a negative B_x and positive B_z component. On the basis of the general solar wind flow and magnetosheath flow [*Spreiter and Stahara*, 1985], the most likely scenario for the magnetic field topology is illustrated in Figure 11. POLAR is on magnetosheath magnetic field lines that are connected to the quasi-parallel bow shock (cf. Figure 10). Energetic ions produced at the shock follow field lines, reach POLAR and are detected by the CAMMICE instrument. This magnetic topology also appears in the global hybrid simulations results (N. Omidi, private communication). For the second interval of intense energetic ion flux, magnetosheath magnetic field B_x and B_z components reverse the sign but the magnetic topology remains similar. POLAR is again on a field line connected to the quasi-parallel bow shock and observes intense energetic ions. On the other hand between the two intervals of enhanced energetic ion flux, θ_{Bx} is very large and POLAR is on field lines connected to the quasi-perpendicular shock and detects very weak energetic ion flux.
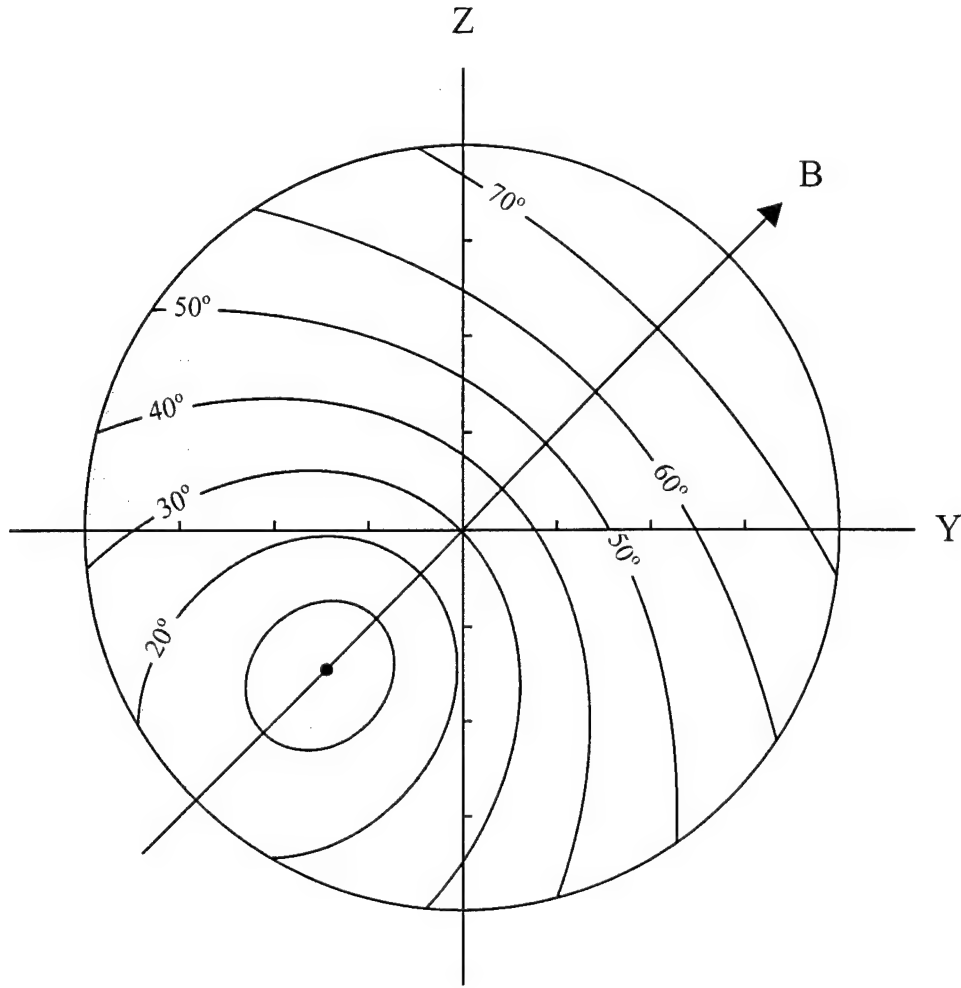
Figure 10. Projection of the dayside bow shock surface onto the y-z plane using the Fairfield model [1971]. Contours of constant θ_{Bn} are calculated for IMF $(B_x, B_y, B_z) = (-13.3, 5.5, 5.5)$ nT with $\theta_{Bx} = 30.3°$. The shaded region is the quasi-parallel shock located at the most part of the southern hemisphere and part of the northern hemisphere.
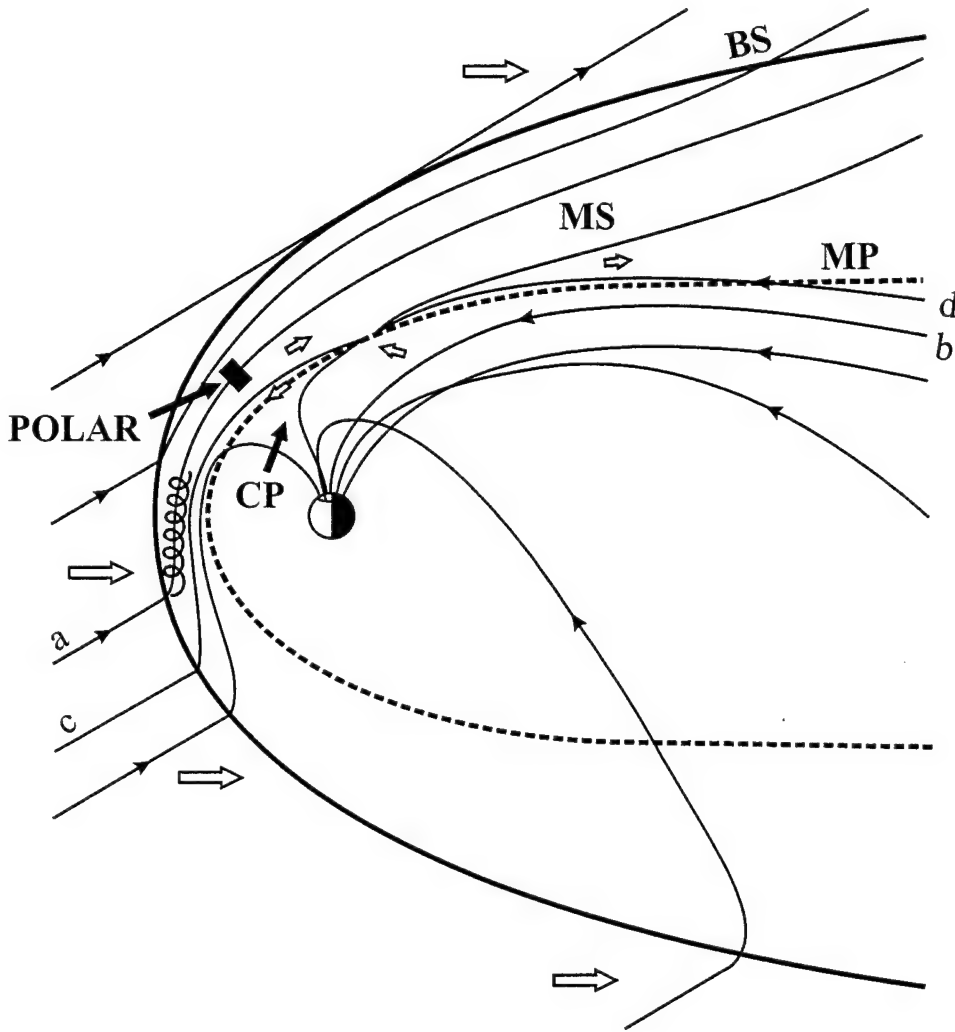
Figure 11. Schematic of the geospace showing the bow shock (BS), magnetosheath (MS), magnetopause (MP), cusp (CP), and the POLAR location. POLAR is in the magnetosheath upstream from the cusp and on magnetic field lines connected to the quasi-parallel bow shock, observing the tailward-streaming energetic ions that are accelerated at the quasi-parallel shock. The magnetosheath field orientation is northward and antisunward in favor of high-latitude reconnection, poleward of the cusp and energetic magnetosheath ions can then directly enter the cusp along the interconnected field lines (e.g., field line c).

Because the observed energetic ions have a very high speed parallel to the magnetic field line, it takes less than 1 min for them to travel from the quasi-parallel bow shock to the POLAR location in the magnetosheath. The solar wind propagation time from the WIND satellite to the bow shock is about 29 min in the interval selected for the correlation analysis. However, the associated time lag for the best correlation between the energetic ion flux and θ_{Bx} is about 36-37 min that is 7-8 min more than the above solar wind propagation time. This time difference can be attributed to the growth time for the energetic ions at the bow shock. As bow shock changes from the quasi-perpendicular to the quasi-parallel geometry, a growth time of $\sim$10 min is required for enhanced 50-200 keV ions [e.g., *Scholer et al.*, 1980; *Mitchell and Roelof*, 1983]. Taking into account the uncertainty of a few minutes (time aliasing) from the CAMMICE detector sampling time, the above time difference is consistent with the early finding of the average growth time.

There is little doubt that majority of magnetosheath energetic ions came from the quasi-parallel bow shock during this event. Since He^{+2} ions are exclusively from the Sun not the ionosphere, they are a part of the solar wind ions accelerated at the quasi-parallel shock not the leaked magnetospheric ions and then transported to the magnetosheath. The remarkable similarity between the magnetosheath energetic H^+ and He^{+2} ions in the spectral shape, correlation coefficient curves, and angular distribution suggests that energetic H^+ ions are likely the solar wind protons accelerated at the quasi-parallel shock and then transported to the magnetosheath just like He^{+2}. Magnetospheric contribution to the magnetosheath energetic ions has to be very minor. The simultaneously enhanced low-frequency waves associated with the magnetosheath energetic ions (Plate 1) are likely from the quasi-parallel bow shock as the energetic ions [e.g., *Luhmann et al.*, 1986; *Möbius et al.*, 1987]. These magnetosheath energetic ions on field lines close to the bow shock eventually cross the shock and escape into the interplanetary medium before field lines are connected to the geomagnetic field lines following magnetic reconnection. When POLAR was upstream from the cusp in the magnetosheath and magnetosheath field had a negative B_x and positive B_z, according to the anti-parallel merging hypothesis the reconnection site was probably at the high-latitude magnetopause poleward of the cusp [*Crooker*, 1979]. Magnetosheath field lines would be connected to the cusp field line and energetic ions produced at the quasi-parallel shock would then enter the cusp along the open field lines (e.g., field line c in Figure 11). These POLAR observations of magnetosheath energetic ions support the hypothesis of bow shock source of CEP's [*Chang et al.*, 1998].

7. Summary and Conclusions

We have presented plasma and magnetic field observations from NASA GGS/POLAR and WIND satellites during the May 4, 1998 magnetic storm event. POLAR was at the dayside magnetosheath in the northern hemisphere and observed energetic (41.1-193.4 keV/e) ion fluxes with large temporal variations (maximum to minimum flux ratio $\sim$100). Their intensity is controlled by the bow shock magnetic geometry. These ions appear to be from the bow shock accelerated ions, not from the magnetosphere based on the following results.

1. POLAR observed distinct ion composition ($O^{<+3}$) and different relative abundance of ions (H^+, He^{+2}, and $O^{>+2}$) in the plasma sheet and magnetosheath. Magnetosheath energetic ions are of solar wind origin.

2. The magnetosheath ion energy spectra are continuous with a spectral break at about 41.1 keV/e for all three ion species, resembling those at the quasi-parallel bow shock. Spectral shape for energetic H^+ and He^{+2} are nearly identical.

3. These magnetosheath energetic ions flow antisunward away from the bow shock along the magnetic field lines. Angular distributions for H^+ and He^{+2} are very similar.

4. Correlation coefficient for the magnetosheath ion flux and the IMF cone angle (θ_{Bx}) depends on the ion energy and time lag for θ_{Bx}. For energy above the spectral break, ion flux and θ_{Bx} offset 36-37 min are strongly anti-correlated, below this energy little correlation.

5. Correlation coefficient curves as a function of the time lag peak at 36-37 min. This lag is consistent with the solar wind propagation time estimated by four different methods plus an allowance for the energization time of the energetic ion fluxes at the quasi-parallel bow shock.

6. Correlation coefficient curves for H^+ and He^{+2} with energy above the spectral break are nearly identical.

7. When POLAR was on field lines connected to the quasi-parallel bow shock, it observed intense energetic ion fluxes. When it was on field lines connected to the quasi-perpendicular bow shock, little energetic ions were observed.

These results can be easily understood by the first-order Fermi acceleration process at the quasi-parallel bow shock. While magnetosheath magnetic field was northward and antisunward in favor of the high-latitude reconnection poleward of the cusp, energetic magnetosheath ions upstream from the cusp were streaming tailward in the magnetic field direction. As the field lines convected and were interconnected with the geomagnetic field lines, energetic magnetosheath ions on these field lines would travel along the interconnected field lines into the cusp. These magnetosheath energetic ion observations support the model of the bow shock source of CEP's [*Chang et al.*, 1998]. Follow-up studies of analyzing multi-satellite observations at the bow shock and in the

cusp, self-consistent global hybrid simulations, and MHD modeling are underway.

References

Asbridge, J. R., S. J. Bame, J. B. Strong, Outward flow of protons from the Earth's bow shock, *J. Geophys. Res.*, *73*, 5777, 1968.

Asbridge, J. R., S. J. Bame, J. T. Gosling, G. Paschmann, and N. Sckopke, Energetic plasma ions within Earth's magnetosheath, *Geophys. Res. Lett.*, *5*, 953, 1978.

Blake, J. B., J. F. Fennell, L. M. Friesen, B. M. Johnson, W. A. Kolasinski, D. J. Mabry, J. V. Osborn, S. H. Penzin, E. R. Schnauss, H. E. Spence, E. N. Baker, R. Belian, T. A. Fritz, W. Ford, B. Laubscher, R. Stiglich, R. A. Baraze, M. F. Hilsenrath, W. L. Imhof, J. R. Kilner, J. Mobilia, D. H. Voss, A. Korth, M. GüLL, K. Fisher, M. Grande, and D. Hall, CEPPAD comprehensive energetic particle and pitch angle distribution experiment on POLAR, *Space Sci. Rev.*, *71*, 531, 1995.

Bonifazi, C., and G. Moreno, Reflected and diffuse ions backstreaming from the Earth's bow shock, *J. Geophys. Res.*, *86*, 4405, 1981.

Chang, S.-W., J. D. Scudder, S. A. Fuselier, J. F. Fennell, K. J. Trattner, J. S. Pickett, H. E. Spence, J. D. Menietti, W. K. Peterson, R. P. Lepping, and R. Friedel, Cusp energetic ions: A bow shock source, *Geophys. Res. Lett.*, *25*, 3729, 1998.

Crooker, N. R., Dayside merging and cusp geometry, *J. Geophys. Res.*, *84*, 951, 1979.

Crooker, N. R., T. E. Eastman, L. A. Frank, E. J. Smith, and C. T. Russell, Energetic magnetosheath ions and the interplanetary magnetic field orientation, *J. Geophys. Res.*, *86*, 4455, 1981.

Ellison, D. C., Shock acceleration of diffuse ions at the Earth's bow shock: Acceleration efficiency and A/Z enhancement, *J. Geophys. Res.*, *90*, 29, 1985.

Ellison, D. C., E. Möbius, and G. Paschmann, Particle injection and acceleration at Earth's bow shock: Comparison of upstream and downstream events, *Astrophys. J.*, *352*, 376, 1990.

Fairfield, D. H., Average and unusual locations of the Earth's magnetopause and bow shock, *J. Geophys. Res.*, *76*, 6700, 1971.

Fuselier, S. A., Energetic magnetospheric protons in the plasma depletion layer, *J. Geophys. Res.*, *97*, 13,759, 1992.

Fuselier, S. A., A comparison of energetic ions in the plasma depletion layer and the quasi-parallel magnetosheath, *J. Geophys. Res.*, *99*, 5855, 1994.

Fuselier, S. A., D. M. Klumpar, and E. G. Shelley, On the origins of energetic ions in the Earth's dayside magnetosheath, *J. Geophys. Res.*, *96*, 47, 1991.

Fuselier, S. A., M. F. Thomsen, F. M. Ipavich, and W. K. H. Schmidt, Suprathermal He^{2+} in the Earth's foreshock region, *J. Geophys. Res.*, *100*, 17,107, 1995.

Gosling, J. T., M. F. Thomsen, S. J. Bame, and C. T. Russell, On the source of diffuse, suprathermal ions observed in the vicinity of the Earth's bow shock, *J. Geophys. Res.*, *94*, 3555, 1989.

Greenstadt, E. W., Oblique, parallel, and quasi-parallel morphology of collisionless shocks, in *Collisionless Shocks in the Heliosphere: Reviews of Current Research, Geophys. Monogr. Ser., vol. 35*, edited by B. T. Tsurutani and R. G. Stone, p. 253, AGU, Washington D. C., 1985.

Greenstadt, E. W., C. T. Russell, and M. Hoppe, Magnetic field orientation and suprathermal ion streams in the Earth's foreshock, *J. Geophys. Res., 85*, 3473, 1980.

Hones, E. W., Jr., S.-I. Akasofu, S. J. Bame, and S. Singer, Outflow of plasma from the magnetotail into the magnetosheath, *J. Geophys. Res., 77*, 6688, 1972.

Ipavich, F. M., A. B. Galvin, G. Gloeckler, M. Scholer, and D. Hovestadt, A statistical survey of ions observed upstream of the Earth's bow shock: Energy spectra, composition, and spatial variation, *J. Geophys. Res., 86*, 4337, 1981.

Lee, M. A., Coupled hydromagnetic wave excitation and ion acceleration upstream of the Earth's bow shock, *J. Geophys. Res., 87*, 5063, 1982.

Lepping, R. P., M. H. Acūna, L. F. Burlaga, W. M. Farrell, L. A. Slavin, K. H. Schatten, F. Mariani, N. F. Ness, F. M. Neubauer, Y. C. Whang, J. B. Byrnes, R. S. Kennon, P. V. Panetta, J. Scheifele, and E. M. Worley, The WIND magnetic field investigation, *Space Sci. Rev., 71*, 207, 1995.

Lin, R. P., C.-I. Meng, and K. A. Anderson, 30- to 100-keV protons upstream from the Earth's bow shock, *J. Geophys. Res., 79*, 489, 1974.

Lin, R. P., K. A. Anderson, S. Ashford, C. Carlson, D. Curtis, R. Ergun, D. Larson, J. McFadden, M. McCarthy, G. K. Parks, H. Réme, J. M. Bosqued, J. Coutelier, F. Cotin, C. d'Uston, W.-P. Wenzel, T. R. Sanderson, J. Henrion, J. C. Ronnet, and G. Paschmann, A three-dimensional plasma and energetic particle investigation for the wind spacecraft, *Space Sci. Rev., 71*, 125, 1995.

Luhmann, J. G., R. J. Walker, C. T. Russell, J. R. Spreiter, S. S. Stahara, and D. H. Williams, Mapping the magnetosheath field between the magnetopause and the bow shock: Implications for magnetospheric particle leakage, *J. Geophys. Res., 89*, 6829, 1984.

Luhmann, J. G., C. T. Russell, and R. C. Elphic, Spatial distributions of magnetic field fluctuations in the dayside magnetosheath, *J. Geophys. Res., 91*, 1711, 1986.

Mitchell, D. G., and E. C. Roelof, Dependence of 50-keV upstream ion events at IMP 7&8 upon magnetic field bow shock geometry, *J. Geophys. Res., 88*, 5623, 1983.

Möbius, E., D. Hovestadt, B. Klecker, M. Scholer, F. M. Ipavich, C. W. Carlson, and R. P. Lin, A burst of energetic O^+ ions during an upstream particle event, *Geophys. Res. Lett., 13*, 1372, 1986.

Möbius, E., M. Scholer, N. Sckopke, H. Lühr, G. Paschmann, and D. Hovestadt, The distribution function of diffuse ions and the magnetic field power spectrum upstream of Earth's bow shock, *Geophys. Res. Lett., 14*, 681, 1987.

Ogilvie, K. W., D. J. Chornay, R. J. Fitzenreiter, F. Hunsacker, J. Keller, J. Lobell, G. Miller, J. D. Scudder, E. C. Sittler Jr., R. b. Torbert, D. Bodet, G. Needell, A. J. Lazarus, J. T. Steinberg, J. H. Tappan, A. Mavretic, and E. Gergin, SWE, a comprehensive plasma instrument for the WIND spacecraft, *Space Sci. Rev., 71,* 55, 1995.

Paschmann, G., N. Sckopke, S. J. Bame, J. R. Asbridge, J. T. Gosling, C. T. Russell, and E. W. Greenstadt, Association of low-frequency waves with suprathermal ions in the upstream solar wind, *Geophys. Res. Lett., 6,* 209, 1979.

Russell, C. T., R. C. Snare, J. D. Means, D. Pierce, D. Dearborn, M. Larson, G. Barr, and G. Le, The GGS/POLAR magnetic field investigation, *Space Sci. Rev., 71,* 563, 1995.

Russell, C. T., G. Le, P. Chi, X.-W. Zhou, J.-H. Shue, S. M. Petrinec, P. Song, F. R. Fenrich, and J. G. Luhmann, The extreme compression of the magnetosphere on May 4, 1998, as observed by the POLAR spacecraft, *Adv. Space Res.,* in press, 1999.

Sarris, E. T., S. M. Krimigis, and T. P. Armstrong, Observations of magnetospheric bursts of high-energy protons and electrons at $\sim$35 R_E with Imp 7, *J. Geophys. Res., 81,* 2341, 1976.

Scholer, M., F. M. Ipavich, G. Gloeckler, and D. Hovestadt, Conditions for acceleration of energetic ions $\geq$ 30 keV associated with the Earth's bow shock, *J. Geophys. Res., 85,* 4602, 1980.

Scholer, M., F. M. Ipavich, G. Gloeckler, D. Hovestadt, and B. Klecker, Leakage of magnetospheric ions into the magnetosheath along reconnected field lines at the dayside magnetopause, *J. Geophys. Res., 86,* 1299, 1981.

Scholer, M., E. Möbius, L. M. Kistler, B. Klecker, and F. M. Ipavich, Multispacecraft observations of energetic ions upstream and downstream of the bow shock, *Geophys. Res. Lett., 16,* 571, 1989.

Scudder, J., D. L. Lind, and K. W. Ogilvie, Electron observations in the solar wind and magnetosheath, *J. Geophys. Res., 78,* 6535, 1973.

Scudder, J. D., F. Hun sacker, G. Miller, J. Lobell, T. Zawistowski, K. Ogilvie, J. Keller, D. Chornay, F. Herrero, R. Fitzenreiter, D. Fairfield, J. Needell, D. Bodet, J. Googins, C. Kletzing, R. Torbert, J. Vandiver, R. Bentley, W. Fillius, C. McIlwain, E. Whipple, and A. Korth, Hydra-A 3-dimensional electron and ion hot plasma instrument for the POLAR spacecraft of the GGS mission, *Space Sci. Rev., 71,* 459, 1995.

Scudder, J. D., P. A. Puhl-Quinn, F. S. Mozer, K. W. Ogilvie, and C. T. Russell, Generalized Walén tests for rotational discontinuities using electron flow velocities, *J. Geophys. Res.,* in press, 1999a.

Scudder, J. D., P. A. Puhl-Quinn, F. S. Mozer, K. W. Ogilvie, and C. T. Russell, Generalized Walén tests for the May 4, 1998 storm event, *J. Geophys. Res.,* in preparation, 1999b.

Scudder, J. D., and A. Hull, Bow shock structure, *J. Geophys. Res.,* in preparation, 1999c.

Scudder, J. D., and C. T. Russell, Plasma observations on May 4, 1998, *J. Geophys. Res.,* in preparation, 1999d.

Sibeck, D. G., R. W. McEntire, A. T. Y. Lui, R. E. Lopez, A. M. Krimigis, R. B. Decker, L. J. Zanetti, and T. A. Potemra, Energetic magnetospheric ions at the dayside magnetopause: Leakage or merging?, *J. Geophys. Res., 92,* 12,097, 1987.

Speiser, T. W., D. J. Williams, and H. A. Garcia, Magnetospherically trapped ions as a source of magnetosheath energetic ions, *J. Geophys. Res., 86,* 723, 1981.

Spreiter, J. R., and S. S. Stahara, Magnetohydrodynamic and gasdynamic theories for planetary bow waves, in *Collisionless Shocks in the Heliosphere: Reviews of Current Research, Geophys. Monogr. Ser., vol. 35,* edited by B. T. Tsurutani and R. G. Stone, p. 85, AGU, Washington D. C., 1985.

Trattner, K. J., E. Möbius, M. Scholer, B. Klecker, M. Hilchenbach, and H. Lühr, Statistical analysis of diffuse ion events upstream of the Earth's bow shock, *J. Geophys. Res., 99,* 13,389, 1994.

West, H. I., Jr., and R. M. Buck, Observations of >100-keV protons in the Earth's magnetosheath, *J. Geophys. Res., 81,* 569, 1976.

Wilken, B., W. Weiss, D. Hall, M. Grande, F. Soraas, and J. F. Fennell, Magnetospheric ion composition spectrometer onboard the CRRES Spacecraft, *Journal Spacecraft and Rockets, 29,* 585, 1992.

Zwan, B. J., and R. A. Wolf, Depletion of solar wind plasma near a planetary boundary, *J. Geophys. Res., 81,* 1636, 1976.

LABORATORY OPERATIONS

The Aerospace Corporation functions as an "architect-engineer" for national security programs, specializing in advanced military space systems. The Corporation's Laboratory Operations supports the effective and timely development and operation of national security systems through scientific research and the application of advanced technology. Vital to the success of the Corporation is the technical staff's wide-ranging expertise and its ability to stay abreast of new technological developments and program support issues associated with rapidly evolving space systems. Contributing capabilities are provided by these individual organizations:

Electronics and Photonics Laboratory: Microelectronics, VLSI reliability, failure analysis, solid-state device physics, compound semiconductors, radiation effects, infrared and CCD detector devices, data storage and display technologies; lasers and electro-optics, solid state laser design, micro-optics, optical communications, and fiber optic sensors; atomic frequency standards, applied laser spectroscopy, laser chemistry, atmospheric propagation and beam control, LIDAR/LADAR remote sensing; solar cell and array testing and evaluation, battery electrochemistry, battery testing and evaluation.

Space Materials Laboratory: Evaluation and characterizations of new materials and processing techniques: metals, alloys, ceramics, polymers, thin films, and composites; development of advanced deposition processes; nondestructive evaluation, component failure analysis and reliability; structural mechanics, fracture mechanics, and stress corrosion; analysis and evaluation of materials at cryogenic and elevated temperatures; launch vehicle fluid mechanics, heat transfer and flight dynamics; aerothermodynamics; chemical and electric propulsion; environmental chemistry; combustion processes; space environment effects on materials, hardening and vulnerability assessment; contamination, thermal and structural control; lubrication and surface phenomena.

Space Science Applications Laboratory: Magnetospheric, auroral and cosmic ray physics, wave-particle interactions, magnetospheric plasma waves; atmospheric and ionospheric physics, density and composition of the upper atmosphere, remote sensing using atmospheric radiation; solar physics, infrared astronomy, infrared signature analysis; infrared surveillance, imaging, remote sensing, and hyperspectral imaging; effects of solar activity, magnetic storms and nuclear explosions on the Earth's atmosphere, ionosphere and magnetosphere; effects of electromagnetic and particulate radiations on space systems; space instrumentation, design fabrication and test; environmental chemistry, trace detection; atmospheric chemical reactions, atmospheric optics, light scattering, state-specific chemical reactions and radiative signatures of missile plumes.

Center for Microtechnology: Microelectromechanical systems (MEMS) for space applications; assessment of microtechnology space applications; laser micromachining; laser-surface physical and chemical interactions; micropropulsion; micro- and nanosatellite mission analysis; intelligent microinstruments for monitoring space and launch system environments.

Office of Spectral Applications: Multispectral and hyperspectral sensor development; data analysis and algorithm development; applications of multispectral and hyperspectral imagery to defense, civil space, commercial, and environmental missions.

THE AEROSPACE CORPORATION

2350 E. El Segundo Boulevard
El Segundo, California 90245-4691
U.S.A.